Compliance Error Compensation based on Reduced Model for Industrial Robots

Shamil Mamedov, Dmitry Popov, Stanislav Mikhel and Alexandr Klimchik
Institute of Robotics, Innopolis University, Universitetskaya Str. 1, Innopolis, Russia

Keywords: Elastostatics, Virtual Joint Method, Industrial Manipulators, Machining, Deflection Compensation.

Abstract: In the near future industrial manipulators can completely replace bulky and expensive CNC machines. The only issue that stands in a way of this transition is low stiffness of industrial robots. However, a lot of research is going on in this area with the focus on developing an accurate stiffness model of the robot and embedding it into the control scheme. The majority of the stiffness models include stiffness of the links as well as joints even though typically complete link parameters are not provided by the robot manufacturers. Therefore, it is of great importance to understand how accurately a reduced stiffness model which takes into account only joint stiffness can replicate the results of the full model. In this paper, we focus on analyzing the quantitative difference between these two models using Virtual Joint Modeling method and its effect on trajectory tracking. The systematic analysis demonstrates that reduced stiffness model can quite accurately replicate the full one and with reduced model, up to 95 percent of the end-effector deflection can be compensated so that the average deflection error after compensation is about 0.8 μm tor a typical heavy industrial robot under the loading.

1 INTRODUCTION

Nowadays there is a tendency to replace computer numerical control (CNC) machines with industrial robots as the latter are cheaper and occupy less space. However, due to open-loop chain structure, the stiffness of industrial robots is lower than of CNC machines. Both theoretical and experimental studies show that this ratio can be more than 50 times (Pan et al., 2006). Deformations due to low stiffness lead to poor machining quality and decreased processing efficiency (Zhang et al., 2005). In order to bring accuracy of manipulators close to the accuracy of CNC machines, researchers tend to model robot elasticity and compensate related compliance errors. For the stiffness modeling three main approaches are distinguished in literature: the finite elements analysis (FEA) (Taghaeipour et al., 2010), the matrix structural analysis (MSA) (Martin, 1966) and the virtual joint method (VJM) (Klimchik et al., 2017; Pashkevich et al., 2009; Pashkevich et al., 2011) each of them have their own advantages and disadvantages. Compliance error compensation is a complicated problem since compensation in the Cartesian space is achieved evidentially by the motors located at the joints and naturally, the following question arises: how accurately total compliance – compliance of the links and joints – can be lumped in the joints and dealt with?

To address this issue, the remainder of the paper is organized as follows. Section 2 defines theoretical models used in this paper. Section 3 describes a model of the robot. In Section 4 results of simulations are given. Section 5 provides discussion and Section 6 summarizes main contributions of the paper.

1.1 Related Work

Stiffness modeling of robotic manipulators was initiated in the 1980s by a pioneering work of Salisbury on active stiffness control (Salisbury, 1980). First models were taking into account only joint elasticities and the stiffness parameters were estimated in a straightforward way (Pigoski et al., 1998). Recent developments in this field make it possible to model both joint and link flexibility (Klimchik et al., 2014), resulting in three main approaches mentioned in the previous section. The basic idea behind the FEA is to decompose the physical model of a mechanism into a number of small elements and to introduce compliant relations between adjacent nodes by corresponding stiffness

Mamedov, S., Popov, D., Mikhel, S. and Klimchik, A.
Compliance Error Compensation based on Reduced Model for Industrial Robots.
DOI: 10.5220/0006905701800191
In *Proceedings of the 15th International Conference on Informatics in Control, Automation and Robotics (ICINCO 2018) - Volume 2*, pages 180-191
ISBN: 978-989-758-321-6

matrices (Corradini et al., 2003). Although this method is highly accurate, as a number of finite elements increase limitations of computer memory and high dimension matrix inversion becomes pressing. The MSA uses the main ideas of the FEA but handles large complaint elements which lead to reduced computational efforts (Martin, 1966). Nevertheless, this approach is hardly applicable for the manipulator in the loaded condition (Klimchik et al., 2012). The last method and the one used in this work is the VJM. It is based on the expansion of the traditional rigid-body model of the robotic manipulator with virtual joints corresponding to the compliances of the links and joints (Pashkevich et al., 2009). The use of VJM in justified by its computational efficiency and acceptable accuracy.

The VJM model requires the parameters of virtual springs in order to compensate the end-effector deflections which are a priori unknown. As in case of the model there are several ways to solve this problem. First one is to approximate links by symmetrical beams and use well-known equations to compute the stiffness. But this method is rather an oversimplification of the problem at hand and will not result in accurate deflection compensation. Another approach is to use CAD model of the manipulator (Pashkevich et al., 2011). However, this method is limited due to non-homogeneity and variations in the material properties. Moreover, CAD models are not provided by the robot manufacturers. The last and seemingly the most reliable approach is to exploit model calibration techniques using the data from the real experiments (Alici and Shirinzadeh, 2005; Nubiola and Bonev, 2013). Since the main goal is to compensate the deflections as much as possible the parameters of the virtual springs should be close to the real ones as much as possible, consequently, the method based on the real experiments is used in this work.

Once the full geometric model of the manipulator including stiffness model is known, one can try to compensate the deflections due to link and joint flexibility. There are two main approaches – online and offline compensations. First one involves modification of the control algorithm by tweaking the manipulator inverse/direct kinematics embedded in robot software (Guillo and Dubourg, 2016; Zhang et al., 2005). The second one is to modify the reference trajectory. Usually, robot manufacturers do not provide access to inner control algorithms therefore in most of the cases user is left with the second option. Therefore, it is not surprising that off-line trajectory modifications are mainly applied in the engineering practice (Belchior et al., 2013; Olabi et al., 2012; Ozaki et al., 1991; Popov et al., 2017). Among the most popular implementations of off-line compensation is so-called "mirror technique" (Chen et al., 2013), where the reference and non-compensated trajectories are symmetrical with respect to the desired one.

1.2 Problem Statement

Estimating all the stiffness parameters including both link and joint stiffness's from experiments is a very challenging task as it requires identification of more than 200 parameters for 6 DoF industrial robot. But is it necessary to estimate them all considering possibility to obtain them from the real experimental data (Klimchik et al., 2015). If the overall stiffness of the joints and links are lumped in the joints only how precise the compensation of the end-effector position due to machining or other industrial processes will be? It is the main question of interest of this work which will be systematically analyzed in the following sections.

2 THEORETICAL BACKGROUND

2.1 Virtual Joint Method

VJM is one of the approaches to develop detailed and complete geometric model of the manipulator which provides more accurate estimates of the end-effector position and orientation. To do so, the original model is complemented by virtual joints which describe the elastic deformations of the links. Moreover, virtual springs are included in the actuated joints, in order to take into account the stiffness of the transmission and control loop. As a result, a so-called extended geometric model of the robot is obtained (Eq. (1))

$$\boldsymbol{t} = g(\boldsymbol{q}, \boldsymbol{\theta}) \tag{1}$$

where $\boldsymbol{q}$ is the vector of actuator coordinates and $\boldsymbol{\theta}$ is the vector of virtual joint coordinates. The values of coordinates $\boldsymbol{q}$ are completely defined by the robot controller, while the values of virtual joint coordinates $\boldsymbol{\theta}$ depend on the external loading $\boldsymbol{w}$ applied to the robot end-effector.

Although the mathematical derivation of the expression for deflection and Cartesian stiffness matrix has been shown in several papers, for completeness of the VJM it is provided here as well. Variations in the virtual joint variables $\boldsymbol{\theta}$ generate

the reaction forces/torques in the corresponding links that are evaluated by the generalized Hooke's law for the manipulator in virtual joints space

$$\boldsymbol{\tau}_\theta = \boldsymbol{K}_\theta \boldsymbol{\theta} \tag{2}$$

where $\boldsymbol{\tau}_\theta$ is the vector of torques generated in virtual joints, $\boldsymbol{K}_\theta = diag\left(K_\theta^1, K_\theta^2, \dots, K_\theta^{n_\theta}\right)$ is overall virtual joint stiffness matrix and $\boldsymbol{K}_\theta^{(i)}$ is the spring stiffness matrix of the corresponding link/joint.

By applying the principle of virtual work and assuming that displacements in the virtual joints $\Delta\boldsymbol{\theta}$ are small, we obtain the virtual work done by the external wrench $\boldsymbol{w}$

$$\delta w = (\boldsymbol{w}^T \boldsymbol{J}_\theta)\Delta\boldsymbol{\theta} \tag{3}$$

where $\boldsymbol{J}_\theta = \partial g(\boldsymbol{q}, \boldsymbol{\theta})/\partial\boldsymbol{\theta}$ is the Jacobian matrix with respect to $\boldsymbol{\theta}$.

On the other hand, for the internal forces $\boldsymbol{\tau}_\theta$, the virtual work is equal to

$$\delta w = -\boldsymbol{\tau}_\theta^T \Delta\boldsymbol{\theta} \tag{4}$$

As in the static equilibrium the total virtual work is equal to zero for any virtual displacement, the equilibrium conditions can be derived as

$$\boldsymbol{\tau}_\theta = \boldsymbol{J}_\theta^T \boldsymbol{w} \tag{5}$$

Combining (2), (5) and linearizing (1) around the equilibrium point, the equation for the end-effector deflection can be obtained

$$\Delta\boldsymbol{t} = \boldsymbol{J}_\theta \boldsymbol{K}_\theta^{-1} \boldsymbol{J}_\theta^T \boldsymbol{w} \tag{6}$$

From Eq. (6) an expression for Cartesian stiffness matrix can be extracted

$$\boldsymbol{K}_C = (\boldsymbol{J}_\theta \boldsymbol{K}_\theta^{-1} \boldsymbol{J}_\theta^T)^{-1} \tag{7}$$

The relationship between the Cartesian and joins spaces proposed in (Zargarbashi et al., 2012) is called the conservative congruence transformation (CCT).

2.2 Identification

To estimate the compliances of virtual springs it is more convenient to rewrite Eq. (6) in a form

$$\Delta\boldsymbol{t} = \sum_{i=1}^{n} \left(\boldsymbol{J}_{\theta,i} \boldsymbol{k}_{\theta,i} \boldsymbol{J}_{\theta,i}^T\right) \boldsymbol{w} \tag{8}$$

where n is number of measurements, the matrices $\boldsymbol{k}_{\boldsymbol{\theta}}^{(i)}$ denote the link/joint compliances to be identified, and $\boldsymbol{J}_\theta^{(i)}$ denote sub-Jacobians - $\boldsymbol{J}_\theta = [\boldsymbol{J}_{\theta,1}, \boldsymbol{J}_{\theta,2} \dots]$. Further, to represent the model in a form standard for identification – as a linear function with respect to parameters to be identified, the Eq. (8) is rewritten as

$$\Delta\boldsymbol{t} = \boldsymbol{A}_k(\boldsymbol{q}, \boldsymbol{w})\boldsymbol{k} \tag{9}$$

where $\boldsymbol{A}_k = [\boldsymbol{J}_{\theta,1} \boldsymbol{J}_{\theta,1}^T \boldsymbol{w}, \dots, \boldsymbol{J}_{\theta,n\theta} \boldsymbol{J}_{\theta,n\theta}^T \boldsymbol{w}]$ is so-called observation matrix and $\boldsymbol{k} = \left(\boldsymbol{k}_{\theta,1}, \boldsymbol{k}_{\theta,2}, \dots, \boldsymbol{k}_{\theta,n\theta}\right)^{\boldsymbol{T}}$. The optimization problem for compliance matrix identification is posed as

$$\sum_{i=1}^{m} \|\Delta\boldsymbol{t}_i - \boldsymbol{A}_k(\boldsymbol{q}_i, \boldsymbol{w}_i)\boldsymbol{k}\|^2 \rightarrow \min_{\boldsymbol{k}} \tag{10}$$

where the index i defines the manipulator configuration number.

3 MODEL DESCRIPTION

As it was mentioned before the virtual joint method is the most appropriate method for the manipulator stiffness modeling (Klimchik et al., 2014). In the frame of this approach, several alternative techniques have been proposed. They differ in a number of parameters and dimensions of virtual springs describing the link/joint elastostatic properties. To be more specific, let us consider KUKA KR270 robotic manipulator (Fig. 1) performing any machining operation. It consists of a fixed base, a serial chain of flexible links, a number of flexible actuated joints, the end-effector which is in contact with a workpiece undergoing machining and an external wrench $\boldsymbol{w}$ applied to it due to the technological process. To build full stiffness model of the robot, VJM proposes to model the stiffness of each link with 6 DoF spring, three of which correspond to translation and three to the rotation and the joint with 1 DoF spring positioned along the axis of rotation of the joint (Fig. 2d). In this case stiffness matrix of the manipulator $\boldsymbol{K}_f$ has the dimension 36×36. To use this model, more than 250 parameters should be known (Klimchik et al., 2013). In an ideal scenario, these parameters can be obtained from CAD model of the given robot, however in reality it is hardly possible. Thus, a lot of effort was put in order to construct simpler models which can provide results close enough to full model.

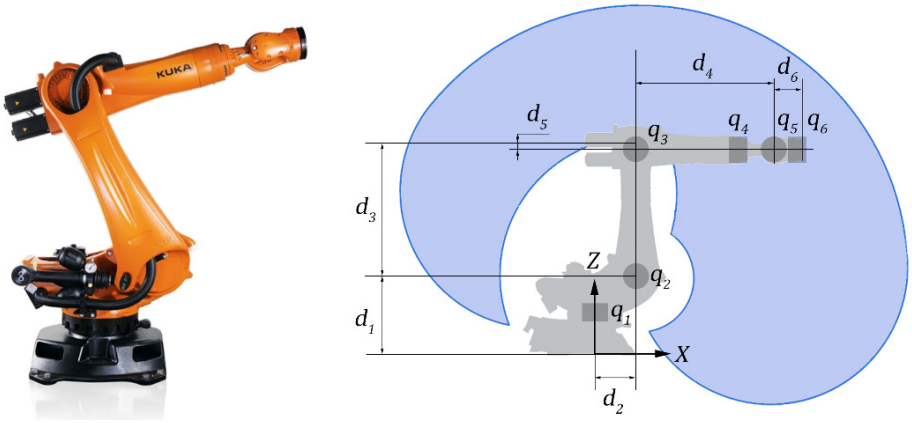

Figure 1: KUKA KR270 and its kinematic scheme with the workspace.

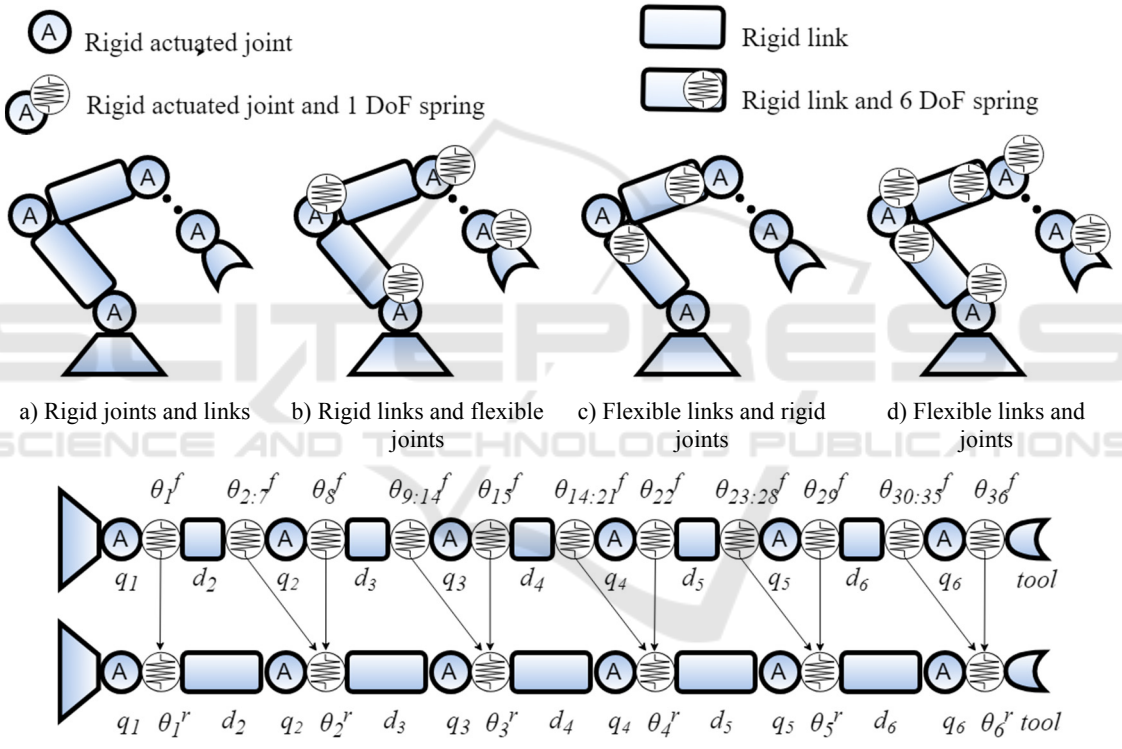

e) Full and reduced models

Figure 2: Possible VJM models for four different cases.

For developing reduced stiffness model there are three main approaches. The first one is used when the stiffness of the joints is much higher than the stiffness of links, therefore the joints can be considered as rigid (Fig. 2c). For this reduced model the stiffness matrix $\boldsymbol{K}_{rl}$ is of dimension 36×36. The second approach is used when the opposite is true i.e. the stiffness of the link is much higher than the stiffness of the joints, thus the links are taken as rigid (Fig. 2b). In this case the stiffness matrix $\boldsymbol{K}_{rj}$ is of dimension 6×6 and diagonal. The last approach is used when the stiffness of the links is higher than of the joints but not negligible. Here, part of a link stiffness is incorporated into the stiffness of the corresponding joint. As in case of $\boldsymbol{K}_{rj}$ the size of the stiffness matrix $\boldsymbol{K}_{rjl}$ is 6×6 and it is diagonal.

The first approach is very rarely used in industrial framework because links of industrial robots are stiff, in addition to that it requires CAD model. Regarding the second approach, links are

usually not rigid enough to neglect them. This model is used in this work to understand the contribution of each elastic component to overall stiffness matrix. The main analysis was performed on full model and reduced model. From now on the reduced model implies the one obtained by the third approach. In the cases when we refer to other reduced models it will be mentioned explicitly.

Table 1: Geometric parameters of the links.

Parameter	Length, m	Outer diameter, m	Inner diameter, m
$\boldsymbol{d_1}$	0.675	0.35	0.30
$\boldsymbol{d_2}$	0.35	0.35	0.30
$\boldsymbol{d_3}$	1.15	0.35	0.30
$\boldsymbol{d_4}$	1.2	0.25	0.20
$\boldsymbol{d_5}$	0.041	0.25	0.20
$\boldsymbol{d_6}$	0.24	0.25	0.20

By using the geometric and virtual springs parameters (Tables 1 and 2) of the KUKA KR270, its extended geometric model can be developed for full (Eq. (11)) and reduced (Eq. (12)) elastostatic models

$$\begin{aligned}\boldsymbol{t}_f = {} & \boldsymbol{T}_z(d_1)\boldsymbol{R}_z(q_1)\boldsymbol{R}_z\left(\theta_1^f\right)\boldsymbol{T}_x(d_2) \\ & \boldsymbol{T}_{3D}\left(\theta_{2:7}^f\right)\boldsymbol{R}_y(q_2)\boldsymbol{R}_y\left(\theta_8^f\right)\boldsymbol{T}_z(d_3) \\ & \boldsymbol{T}_{3D}\left(\theta_{9:14}^f\right)\boldsymbol{R}_y(q_3)\boldsymbol{R}_y\left(\theta_{15}^f\right)\boldsymbol{T}_x(d_4) \\ & \boldsymbol{T}_{3D}\left(\theta_{16:21}^f\right)\boldsymbol{R}_x(q_4)\boldsymbol{R}_x\left(\theta_{22}^f\right)\boldsymbol{T}_z(-d_5) \\ & \boldsymbol{T}_{3D}\left(\theta_{23:28}^f\right)\boldsymbol{R}_y(q_5)\boldsymbol{R}_y\left(\theta_{29}^f\right)\boldsymbol{T}_x(d_6) \\ & \boldsymbol{T}_{3D}\left(\theta_{30:35}^f\right)\boldsymbol{R}_x(q_6)\boldsymbol{R}_x\left(\theta_{36}^f\right)\end{aligned} \quad (11)$$

$$\begin{aligned}\boldsymbol{t_r} = {} & \boldsymbol{T}_z(d_1)\boldsymbol{R}_z(q_1)\boldsymbol{R}_z(\theta_1^r)\boldsymbol{T}_x(d_2)\boldsymbol{R}_y(q_2) \\ & \boldsymbol{R}_y(\theta_2^r)\boldsymbol{T}_z(d_3)\boldsymbol{R}_y(q_3)\boldsymbol{R}_y(\theta_3^r)\boldsymbol{T}_x(d_4) \\ & \boldsymbol{R}_x(q_4)\boldsymbol{R}_x(\theta_4^r)\boldsymbol{T}_z(-d_5)\boldsymbol{R}_y(q_5) \\ & \boldsymbol{R}_y(\theta_5^r)\boldsymbol{T}_x(d_6)\boldsymbol{R}_x(q_6)\boldsymbol{R}_x(\theta_6^r)\end{aligned} \quad (12)$$

where $\boldsymbol{T}_u$ is a homogeneous transformation matrix with translation in u direction, $\boldsymbol{R}_u$ is a homogeneous transformation matrix with rotation about u axis, $\boldsymbol{T}_{3D}$ is a homogeneous transformation matrix with all 6 translation and rotation components. Both models are also presented in Fig. 2e.

Table 2: Joint stiffness values and upper and lower limits.

Joint №	Compliance um/N	Lower limit, deg.	Upper limit, deg.
1	0.4	-179	179
2	0.28	-50	90
3	0.28	-155	120
4	2.5	-350	350
5	2.8	-122	122
6	2	-350	350

Table 3: Identified joints compliances of the manipulator.

Joint №	1	2	3	4	5	6
$\boldsymbol{k_{c,i}}$ $\boldsymbol{\mu m/N}$	0.56	0.30	0.43	2.8	3.2	2.1

3.1 Stiffness Estimation

The process of stiffness identification consists of two steps. First one is displacement modeling. Here it is assumed that both joints and links are elastic and influence the end-effector position. In order to find the value of the displacement, system Jacobian for the given configuration is required (Eq. (6)). It can be obtained from the solution of the forward kinematic problem. If the Jacobian and virtual joint stiffness matrices are known, then the vector of displacement can be calculated using Eq. (8).

The second step is robot calibration. During this step it is assumed that joints are elastic while links are rigid, i.e. try to find an equivalent manipulator with elastic joints that have the same displacement parameters as the initial robot. Thus, only the actuator stiffness values have to be identified.

Identification process requires the measurements of the end-effector in different configurations and under the various force orientation. Mathematical model allows to sequentially check all possible states in robot workspace, but this is not necessary. In experiments, random joint angles were generated and force with arbitrary orientation and a constant value of 10^3 N was applied to the end-effector. The process terminated when the relative error of one iteration was less than a predefined threshold (about 0.01%). Obtained results are represented in Table 3.

Cartesian compliance matrix $\boldsymbol{k_c}$ which is the inverse of the cartesian stiffness matrix, $\boldsymbol{K_c}$ sets the relationship between the generalized displacement of the end-effector and external wrench applied to it (Eq. (6-7)). The problem with $\boldsymbol{k_c}$ is that it has elements with different physical units. It causes difficulties in analyzing compliance of the robot. However, it was shown in (Zargarbashi et al., 2012)

that in machining operations the rotational displacement of the tool can be negligible compared to its translational displacement. Thus, the analysis of generalized end-effector displacement can be reduced to the analysis of its translational displacement, so that Eq. (6) and Eq. (7) combined become:

$$\begin{bmatrix}\Delta \boldsymbol{p}\\ 0\end{bmatrix} = \boldsymbol{k}_c \begin{bmatrix}\boldsymbol{F}\\ 0\end{bmatrix} \quad (13)$$

where $\Delta \boldsymbol{p} = [\Delta p_x \quad \Delta p_y \quad \Delta p_z]^T$ and $\boldsymbol{F} = [F_x \quad F_y \quad F_z]^T$. Compliance matrix $\boldsymbol{k}_c$ can be divided into four submatrices (Guo et al., 2015):

$$\boldsymbol{k}_c = \begin{bmatrix}\boldsymbol{k}_{c,tt} & \boldsymbol{k}_{c,tr}\\ \boldsymbol{k}_{c,tr}^T & \boldsymbol{k}_{c,rr}\end{bmatrix} \quad (14)$$

where $\boldsymbol{k_{c,tt}}$ is the translational compliance submatrix, $\boldsymbol{k_{c,rr}}$ is the rotational compliance submatrix, and $\boldsymbol{k_{c,tr}}$ is the coupling compliance submatrix.

By substituting Eq. (14) into Eq. (13) a direct relationship between $\Delta \boldsymbol{p}$ and $\boldsymbol{F}$ can be obtained

$$\Delta \boldsymbol{p} = \boldsymbol{k}_{c,tt} \boldsymbol{F} \quad (15)$$

Eq. (15) is used further in this paper in order to build deflection maps.

3.2 Deflection Maps

When the joint stiffness values are known, distribution of deflection in the robot workspace (deflection map) can be built. Such maps could be calculated, for example, along the end-effector trajectory or for some workspace plane. Both representations are considered in this work.

There are several problems that can be encountered during these computations. One of them is a robot configuration as it is obvious that parts of the workspace can be reached using several configurations, while other parts only by one combination of joint angles. Each configuration is characterized by its own stiffness, so the question is which one should be used for computation? This problem does not have much sense for the given robot in case of operation in XOY plane because each point can be reached without changing manipulator configuration. But in the orthogonal plane (XOZ) in order to obtain highest or lowest points of workspace configuration must be changed.

For the manipulator used for simulations and represented in Fig. 2, there are two main configurations: "elbow up" – when the angle $\boldsymbol{q_3}$ is negative and "elbow down" – when $\boldsymbol{q_3}$ is positive. In the horizontal plane, for the sake of simplicity, only one of them, "elbow up" is considered as it is more common. In case of the vertical plane, two deflections for different workspaces should be combined. It is assumed that manipulator will operate in optimal mode hence minimal deflection should be chosen in the intersection of two regions.

The second problem is the value and direction of the applied force which could provide the worst result, i.e. maximum deflection. This problem can be solved by exploiting the singular value decomposition (SVD) method (Leon, 1980) applied to the translational compliance submatrix (Eq. (15)).

$$\boldsymbol{k}_{c,tt} = \boldsymbol{U}\boldsymbol{S}\boldsymbol{V}^T \quad (16)$$

where the diagonal elements of $\boldsymbol{S}$ are nonnegative singular values in decreasing order, the columns of $\boldsymbol{U}$ are left singular vectors and columns of $\boldsymbol{V}$ are right singular vectors.

The first element of the matrix $\boldsymbol{S}$ is an absolute value of the maximal deflection obtained under the influence of a unit force (1 N). Direction of this deflection is corresponding left singular vector i.e. first column of matrix $\boldsymbol{V}$. The similar approach was used in (Guo et al., 2015).

4 RESULTS

4.1 Deflection Maps

Deflection maps for the manipulator with the full elastostatic model are shown in Fig. 4. Upper image corresponds to the vertical plane at the 0.5 m level. The map demonstrates radial symmetry, deflection grows with distance and increases from the center to the edges due to increase in the lever length. As in case of the horizontal plane, the deflection increases proportionally to the distance from the origin of the base link due to the same reason. Here no symmetry can be spotted as the second and third joint limits are not symmetrical with respect to the Z axis. Maximum deflection that manipulator undergoes under the unit force applied in the direction leading to maximum deflection for both vertical and horizontal planes is 4 μm. The sudden change of the deflection along X-axis corresponds to the change from the configuration "elbow up" to "elbow down". Deflection maps of the manipulator with the reduced elastostatic model – the model which takes into account only estimated joint elasticities, obtained from the calibration process (Table 3) are shown in Figure 4.

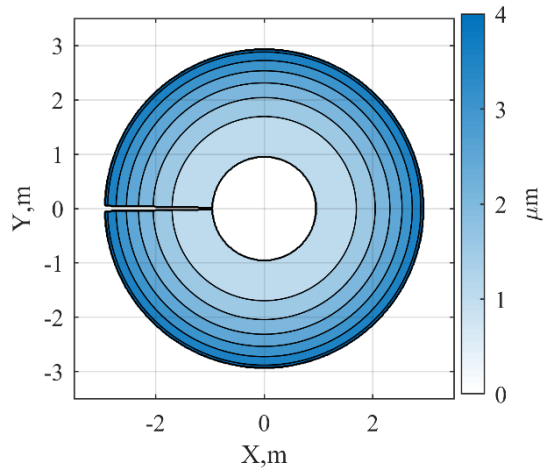

a) Horizontal plane

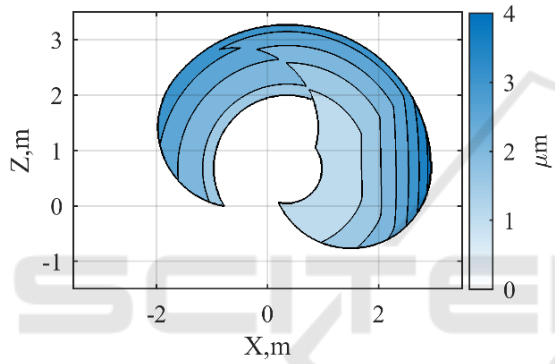

b) Vertical plane

Figure 3: Deflection maps for the manipulator with full elastostatic model.

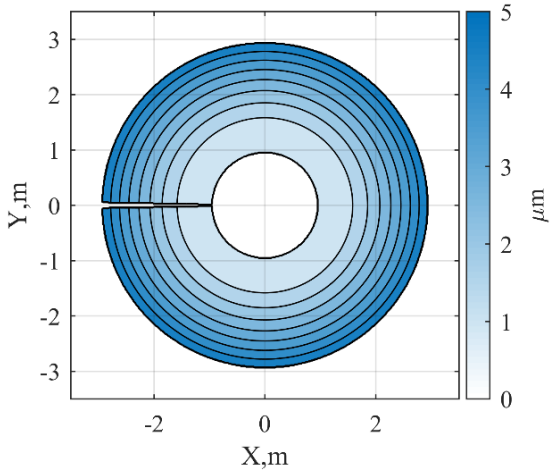

a) Horizontal plane

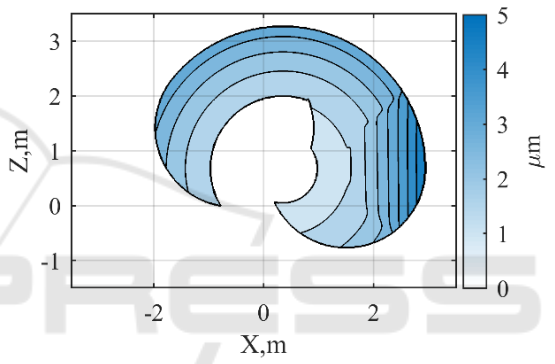

b) Vertical plane

Figure 4: Deflection maps for the manipulator with reduced elastostatic model.

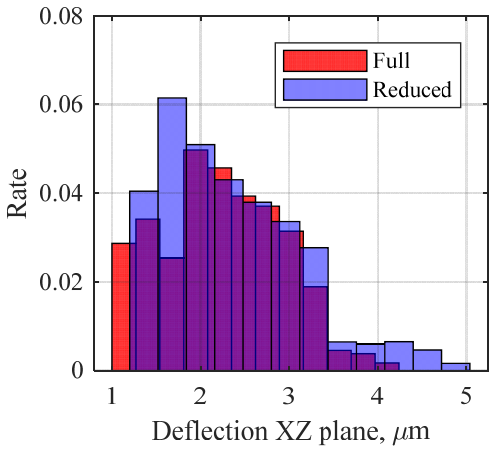

a) Vertical plane

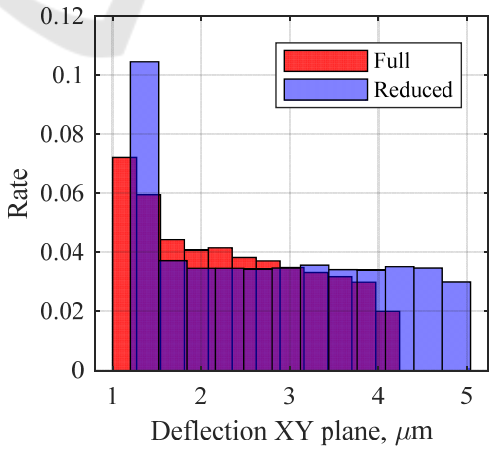

b) Horizontal plane

Figure 5: Error histograms of the full and the reduced models.

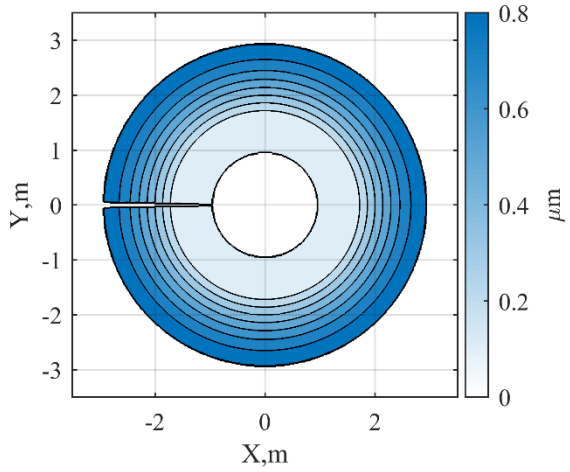

a) Horizontal plane

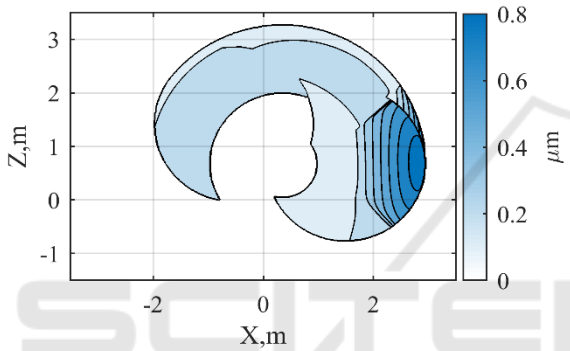

b) Vertical plane

Figure 6: The difference in the deflection maps of the manipulator with full and reduced model.

It is rather obvious that reduced model deflection map is different from the full as the number of elastic elements representing the manipulator is decreased. However, the difference is not significant because experiment based compliance identification of the joint parameters incorporates some of the link parameters. For this reason, the reduced model can provide results accurate enough to be used in the compensation process. To understand the degree of accuracy the difference between full and reduced model deflection maps is provided in the Fig. 6.

Fig. 6 shows that the maximum difference is 0.8 μm (84%) and concentrated on the particular region. It is explained by the chosen approach where we apply unit force along the direction of maximum deflection extracted from the full model as it better describes elasticity of the manipulator. The simple conclusion that can be drawn from the difference map is that the reduced model is very good in recovering the performance of the full model for the setup considered in this paper while requiring many fewer parameters (Fig. 5 demonstrates that error distributions are almost the same).

4.2 Deflection Compensation

In order to find an error of obtained model, we can compare trajectories of the end-effector with and without compensation for some technological process. Assuming that the manipulator has to move along the trajectory, shown in Fig. 7a, 8a under the influence of the force $\boldsymbol{F} = [440, -1370, -635, 0, 0, 0]$, cutting forces caused by machining process (Klimchik et al., 2017). This force makes the trajectory of the end-effector different from the desired one. Depending on the value and the orientation of the applied force, the difference between trajectories can not only be shifted but also has a different shape.

In order to compensate for the difference, the deflection at each point should be found, using reduced stiffness model of the manipulator. At this point, widely used mirroring technique can be utilized for compensation. New compensated trajectory is used as an input of the manipulator control system. The error between desired and obtained trajectories for the robot without compensation in every direction is shown in the Fig. 9b, 10b while the same figure but for the robot with compensation is demonstrated in the Fig. 7c, 8c. Mean and maximum errors for both cases are presented in Table 4 and 5.

Table 4: Max and mean error for circle with 0.01m radius.

Direction	Uncompensated		Compensated	
	Max error, mm	Mean error, mm	Max error, mm	Mean error, mm
X	0.779	0.776	0.114	0.113
Y	1.841	1.825	0.169	0.160
Z	0.639	0.628	0.019	0.017

Table 5: Max and mean error for circle with 0.5m radius.

Direction	Uncompensated		Compensated	
	Max error, mm	Mean error, mm	Max error, mm	Mean error, mm
X	1.072	0.753	0.185	0.111
Y	2.838	1.968	0.622	0.314
Z	1.261	0.701	0.079	0.045

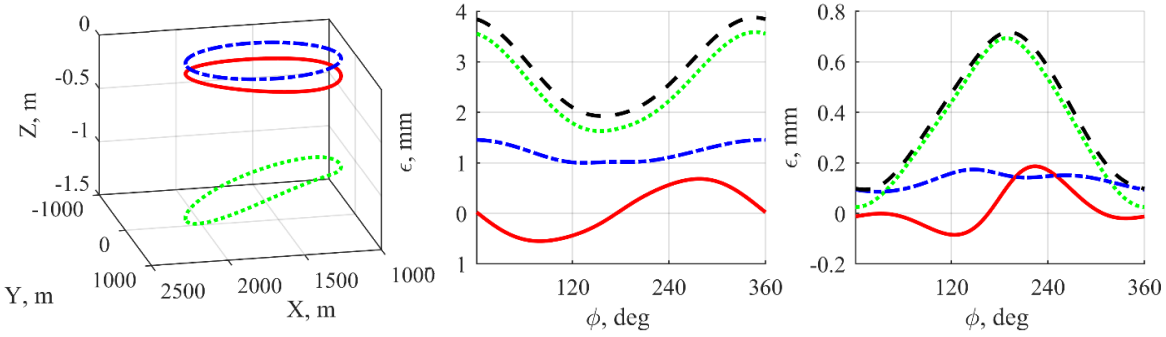

a) Trajectories in the Cartesian space Green dotted circle is uncalibrated trajectory, the blue dash-dot circle is desired trajectory, the red solid circle is a trajectory after calibration process

b) Position error for the uncompensated case. The red solid line is an error in the X direction, Green dotted line is an error in the Y direction, Blue dash-dot line is an error in the Z direction, the Dashed line is error norm

c) Position error for the compensated case. The red solid line is an error in the X direction, Green dotted line is an error in the Y direction, Blue dash-dot line is an error in the Z direction, the Dashed line is error norm

Figure 7: Tool trajectories a circle with 0.5m radius.

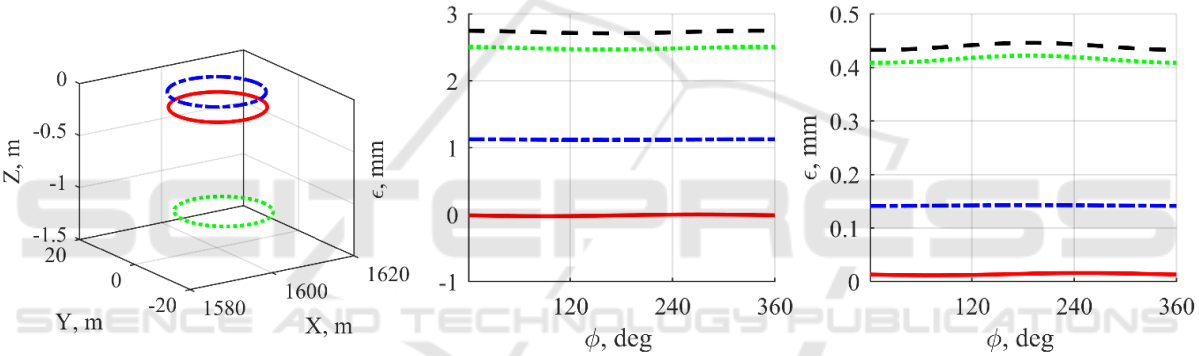

a) Trajectories in Cartesian space Green dotted circle is uncalibrated trajectory, Blue dash-dot circle is desired trajectory, the Red solid circle is a trajectory after calibration process

b) Position error for the uncompensated case. The red solid line is an error in the X direction, Green dotted line is an error in the Y direction, Blue dash-dot line is an error in the Z direction, the Dashed line is error norm

c) Position error for the compensated case. The red solid line is an error in the X direction, Green dotted line is an error in the Y direction, Blue dash-dot line is an error in the Z direction, the Dashed line is error norm

Figure 8: Tool trajectories for a circle with 0.01m radius.

For the small circle trajectory with 0.01m radius, the maximum error is decreased by 85% in X, 91% in Y and 97% in Z directions while for the large circle maximum error is decreased by 83% in X, 78% in Y and 94% in Z directions. At the same time mean error in case of the small circle was reduced by 85%, 91% and 97% in X, Y and Z directions correspondingly, while in case of the large circle mean error was reduced by 85% in X, 84% in Y and 94% in Z directions. To be more concise, the maximum and the mean norms of the error for large circle were decreased by 80% and 84% respectively while for small circle both by 90%. The numbers demonstrate excellent quality of the compensation even though it is based on the reduced model.

5 DISCUSSION

So far, the analysis was conducted for the manipulator having geometrical properties of KUKA KR270. Due to unknown internal structure of its links, to develop full elastostatic model, we roughly approximated all the links with hollow cylinders with a wall thickness of 5cm. Thus, the results hold true for this particular case and are not applicable to

the generic manipulator. To generalize obtained results, first, we define more practical workspace – restricted workspace (Fig. 9), which has the same contour as full one but is smaller as to avoid singularities. Then, we vary the thickness of the walls from one to ten centimeters, to understand how it affects the quality of compensation in full and restricted workspaces.

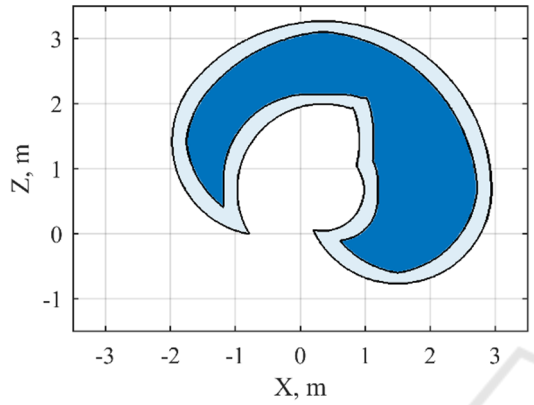

Figure 9: Full and restricted robot workspaces in XZ.

As the thickness of the walls decreases the quality of compensation decreases as well. The efficiency of the compensation for both workspaces is especially sensitive to wall thickness in the range from one to four centimeters (Fig. 10).

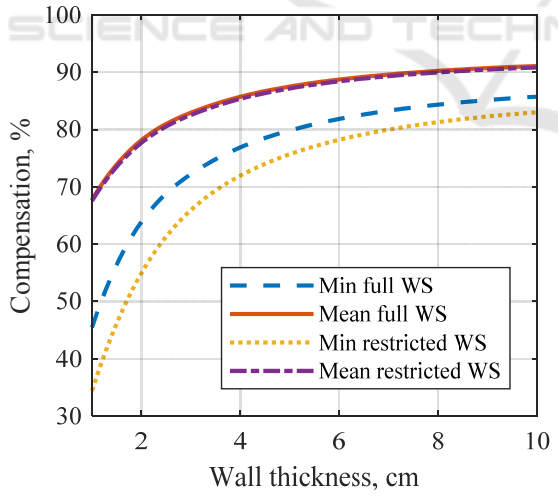

Figure 10: Compensation effectiveness for reduced model depending on link thickness.

To explain this, we can carry out a simple experiment which makes use of the first two reduced models described in Section 3. The experiment is the following, for the whole workspace compute deflections by using full model, a reduced model which assumes that links are rigid and reduced model which assumes that joints are rigid. Then find the mean value of the deflection for all three cases, repeat the procedure for all the given values of wall thickness. The ration between the mean values of a reduced model and the full model will show the contribution of the links or joints to overall deflection (Fig. 11). As reduced models complement each other to the full model, only one of them is plotted and allows to understand the whole picture.

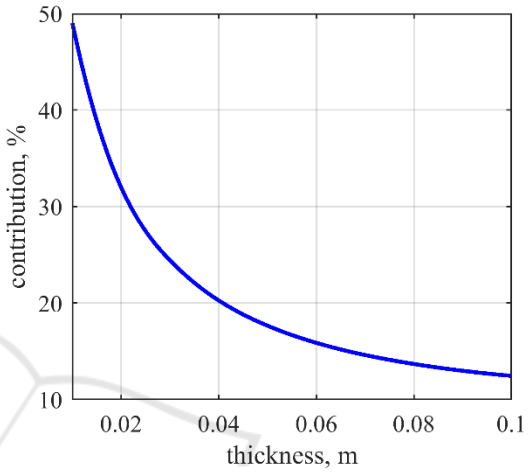

Figure 11: Contribution of the compliance of the links to the overall deflection of the full elastostatic model.

When walls are thin, due to low stiffness they have a great deal of contribution to overall deflection. Although the reduced model used throughout this work accounts for some compliance of the links, it is not enough to provide good quality of compensation.

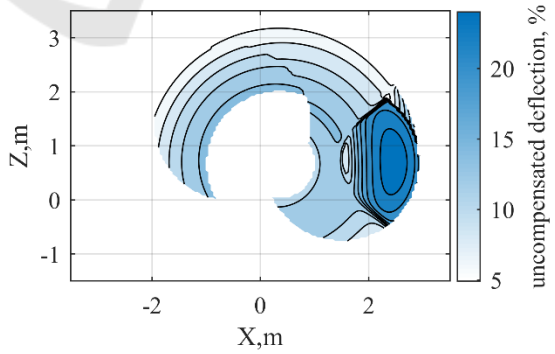

Figure 12: Uncompensated deflection in the vertical plane.

Regarding the Fig. 10, the minimum deflection of the overall workspace is more than of restricted one, this rather unintuitive results can be explained by Fig.12 which shows that the compensation in the regions neglected in restricted workspace was very

good. Nevertheless, the mean value of compensation is almost the same for both workspaces.

There are several remarks to be made. First, for simplicity, we assume that the manipulator does not have gravity compensator. Its presence slightly complicates the analysis by making the stiffness of the second joint a nonlinear function of angle $\boldsymbol{q}_2$ (Klimchik et al., 2013). Second, the metrics used in this work are maximum and mean values of deflection when we analyze workspace, and maximum and mean values of errors in all X, Y and Z direction when we consider the trajectory of the end effector. The usage of other metrics can provide slightly different results. Third, the orientation error is neglected as the level of precision that is discussed in this paper is used in the field of machining and it was shown that for machining operations the rotational displacement of the tool is negligible (Zargarbashi et al., 2012). The last, while performing deflection analysis for overall workspace we did not assume any specific machining operation for the sake of generality and used singular value decomposition to define the direction of maximum deflection for the full model and apply unit force along this direction for both full and reduced model in estimating deflection. However, for a specific machining operation, the analysis can be particularized by defining the force on the end-effector due to machining.

In our simulation we use a large number of configurations and end-effector loads in the identification process, that is hardly implementable in real life scenario. To reduce the number of experiments and preserve resulting accuracy, the design of experiment theory could be used (Klimchik et al., 2015; Klimchik et al., 2012; Wu et al., 2015).

6 CONCLUSIONS

In the majority of the studies focused on deflection compensation of the industrial manipulators, authors assume the links to be rigid. In this work, we focus on understanding when this assumption holds true and in which cases the compliance of the links cannot be neglected. It was shown that when the walls of the links modeled as hollow cylinders are thin (up to 4cm) full elastostatic model should be considered while when they are thick enough (4cm and more) then depending on the actual thickness of the walls reduced model can compensate more than 80% of overall deflections in general.

In our future work, we plan to consider the efficiency of the proposed method in real industrial applications. This will introduce additional difficulties that affect output accuracy like the presence of the measurement noise, greatly reduced a number of experiments, dynamic components that currently is not considered by our model.

ACKNOWLEDGEMENTS

This research has been supported by the grant of Russian Science Foundation №17-19-01740.

REFERENCES

Alici, G., and Shirinzadeh, B., 2005. Enhanced stiffness modeling, identification and characterization for robot manipulators. *IEEE Transactions on Robotics*, *21*, 554–564.

Belchior, J., Guillo, M., Courteille, E., Maurine, P., Leotoing, L., and Guines, D., 2013. Off-line compensation of the tool path deviations on robotic machining: Application to incremental sheet forming. *Robotics and Computer-Integrated Manufacturing*, *29*, 58–69.

Chen, Y., Gao, J., Deng, H., Zheng, D., Chen, X., and Kelly, R., 2013. Spatial statistical analysis and compensation of machining errors for complex surfaces. *Precision Engineering*, *37*, 203–212.

Corradini, C., Fauroux, J., Krut, S., and Company, O., 2003. Evaluation of a 4-Degree of Freedom Parallel Manipulator Stiffness. *Proceedings of the 11th World Congress in Mechanism and Machine Science*, 5.

Guillo, M., and Dubourg, L., 2016. Impact and improvement of tool deviation in friction stir welding: Weld quality and real-time compensation on an industrial robot. *Robotics and Computer-Integrated Manufacturing*, *39*, 22–31.

Guo, Y., Dong, H., and Ke, Y., 2015. Stiffness-oriented posture optimization in robotic machining applications. *Robotics and Computer-Integrated Manufacturing*, *35*, 69–76.

Klimchik, A., Ambiehl, A., Garnier, S., Furet, B., and Pashkevich, A., 2017. Efficiency evaluation of robots in machining applications using industrial performance measure. *Robotics and Computer-Integrated Manufacturing*, *48*, 12–29.

Klimchik, A., Caro, S., and Pashkevich, A., 2015. Optimal pose selection for calibration of planar anthropo-morphic manipulators. *Precision Engineering*, *40*, 214–229.

Klimchik, A., Chablat, D., and Pashkevich, A., 2014. Stiffness modeling for perfect and non-perfect parallel manipulators under internal and external loadings. *Mechanism and Machine Theory*, *79*, 1–28.

Klimchik, A., Furet, B., Caro, S., and Pashkevich, A., 2015. Identification of the manipulator stiffness model parameters in industrial environment. *Mechanism and Machine Theory*, *90*, 1–22.

Klimchik, A., Pashkevich, A., and Chablat, D., 2013. CAD-based approach for identification of elasto-static parameters of robotic manipulators. *Finite Elements in Analysis and Design*, *75*, 19–30.

Klimchik, A., Wu, Y., Caro, S., Furet, B., and Pashkevich, A., 2014. Accuracy improvement of robot-based milling using an enhanced manipulator model. In *Mechanisms and Machine Science* (Vol. 22, pp. 73–81).

Klimchik, A., Wu, Y., Dumas, C., Caro, S., Furet, B., and Pashkevich, A., 2013. Identification of geometrical and elastostatic parameters of heavy industrial robots. In *Proceedings - IEEE International Conference on Robotics and Automation* (pp. 3707–3714).

Klimchik, A., Wu, Y., Pashkevich, A., Caro, S., and Furet, B., 2012. Optimal Selection of Measurement Configurations for Stiffness Model Calibration of Anthropomorphic Manipulators. *Applied Mechanics and Materials*, *162*, 161–170.

Leon, S. J., 1980. *Linear algebra with applications*. Macmillan New York.

Martin, H. C., 1966. *Introduction to matrix methods of structural analysis*. McGraw-Hill.

Nubiola, A., and Bonev, I., 2013. Absolute calibration of an ABB IRB 1600 robot using a laser tracker. *Robotics and Computer-Integrated Manufacturing*, *29*, 236–245.

Olabi, A., Damak, M., Bearee, R., Gibaru, O., and Leleu, S., 2012. Improving the accuracy of industrial robots by offline compensation of joints errors. In *2012 IEEE International Conference on Industrial Technology, ICIT 2012, Proceedings* (pp. 492–497).

Ozaki, T., Suzuki, T., Furuhashi, T., Okuma, S., and Uchikawa, Y., 1991. Trajectory control of robotic manipulators using neural networks. *IEEE Transactions on Industrial Electronics*, *38*, 536–540.

Pan, Z., Zhang, H., Zhu, Z., and Wang, J., 2006. Chatter analysis of robotic machining process. *Journal of Materials Processing Technology*, *173*, 301–309.

Pashkevich, A., Chablat, D., and Wenger, P., 2009. Stiffness analysis of overconstrained parallel manipulators. *Mechanism and Machine Theory*, *44*, 966–982.

Pashkevich, A., Klimchik, A., and Chablat, D., 2011. Enhanced stiffness modeling of manipulators with passive joints. *Mechanism and Machine Theory*, *46*, 662–679.

Pigoski, T., Griffis, M., and Duffy, J., 1998. Stiffness Mappings Employing Different Frames of Reference. *Mechanism and Machine Theory*, *33*, 825–838.

Popov, D., Klimchik, A., and Afanasyev, I., 2017. Design and Stiffness Analysis of 12 DoF Poppy-inspired Humanoid. In *Proceedings of the 14th International Conference on Informatics in Control, Automation and Robotics* (pp. 66–78).

Salisbury, J., 1980. Active stiffness control of a manipulator in cartesian coordinates. *Proc. IEEE Conf. on Decision and Control (CDC)*, *19*, 95–100.

Taghaeipour, A., Angeles, J., and Lessard, L., 2010. Online computation of the stiffness matrix in robotic structures using finite element analysis. *Department of Mechanical Engineering and Centre for Intelligent Machines, McGill University, Montreal*.

Wu, Y., Klimchik, A., Caro, S., Furet, B., and Pashkevich, A., 2015. Geometric calibration of industrial robots using enhanced partial pose measurements and design of experiments. *Robotics and Computer-Integrated Manufacturing*, *35*, 151–168.

Zargarbashi, S. H. H., Khan, W., and Angeles, J., 2012. Posture optimization in robot-assisted machining operations. *Mechanism and Machine Theory*, *51*, 74–86.

Zhang, H., Wang, J., Zhang, G., Gan, Z., Pan, Z., Cui, H., and Zhu, Z., 2005. Machining with flexible manipulator: toward improving robotic machining performance. In *Advanced Intelligent Mechatronics. Proceedings, 2005 IEEE/ASME International Conference on* (pp. 1127–1132).